Supplementary Information:

Unique Size-Dependent Nanocatalysis Revealed at Single Atomically Precise Gold Cluster Level

Yuwei Zhang[a†], Ping Song[a†], Tiankai Chen[b], Xiaodong Liu[a, c], Tao Chen[a, c], Zhemin Wu[d], Yong Wang[d], Jianping Xie[b,*], Weilin Xu[a,*]

Affiliations:

[a]State Key Laboratory of Electroanalytical Chemistry, &Jilin Province Key Laboratory of Low Carbon Chemical Power, Changchun Institute of Applied Chemistry, Chinese Academy of Science, 5625 Renmin Street, Changchun 130022, China.

[b]Department of Chemical and Biomolecular Engineering, National University of Singapore, 4 Engineering Drive 4, 117585, Singapore.

[c]University of Chinese Academy of Science, Beijing, 100049, China.

[d]Center of Electron Microscopy and State Key Laboratory of Silicon Materials, School of Materials Science and Engineering, Zhejiang University, Hangzhou 310027, P. R. China.

[†]These authors contributed equally to this work.

[*]To whom correspondence should be addressed. E-mail: weilinxu@ciac.ac.cn (W. X.); chexiej@nus.edu.sg (J. X.)

1. Materials and methods

Gold(III) chloride trihydrate ($HAuCl_4 \cdot 3H_2O$), 3-mercaptopropionic acid (MPA) and 6-Mercaptohexanoic acid (MHA) were purchased from Sigma-Aldrich. NaOH was purchased from Merck, and carbon monoxide (CO) was provided by Singapore Oxygen Air Liquide (SOXAL). Ultrapure water (Milli-Q) with a resistivity of 18.2 MΩ·cm was used as solvent for the synthesis of Au clusters.

The MPA protected Au nanoclusters were synthesized based on a reported protocol.[S1] Aqueous solution of $HAuCl_4$ (12.5 mL, 20 mM) and MPA (10.0 mL, 50 mM) were mixed with 227.5 mL water inside a 500-mL flask. After 2 min of vigorous stirring, 1 M NaOH solution was added to bring the solution to a certain pH value: to synthesize $Au_{15}(MPA)_{13}$, $Au_{18}(MPA)_{14}$ and $Au_{25}(MPA)_{18}$, 1.75 mL, 2.25 mL and 5.0 mL 1 M NaOH are added, respectively, to bring the pH of the solution to about 10.0, 11.0 and 12.0, respectively. 1 bar of CO is then bubbled to the solution for 2 minutes, followed by the reactor sealed airtight. The reaction solutions were stirred at 500 rpm for 24 h before sample collection. The MHA protected Au_{25} clusters ($Au_{25}(MHA)_{18}$) were synthesized in a similar way.[S2]

www.pnas.org/cgi/doi/10.1073/pnas.1805711115

UV-Vis absorption spectra were measured on a Shimadzu UV-1800 photospectrometer. Electrospray ionization spectrometry (ESI-MS) was conducted on a Bruker MicroTOF-Q ESI time-of-flight system operating at negative ion mode. The sample injection rate was 180 $\mu L \cdot h^{-1}$, and the ESI source was operated with capillary voltage 4 kV, nebulizer 1.5 bar, and dry gas 4 $L \cdot min^{-1}$ at 120 °C.

The morphology and dimensions of as-prepared Au samples were obtained from transmission electron microscopy (TEM), a JEM-2100F microscopy with an accelerating voltage of 200 kV. Sub-angstrom resolution HAADF STEM images were obtained from a FEI TITAN ChemiSTEM equipped with a CEOS (Heidelburg, Ger) probe corrector, operating at 200 kV. X-ray photoelectron spectroscopic (XPS) measurements were performed on an AXIS Ultra DLD (Kratos company) using a monochromic Al X-ray source.

Single-molecule nanocatalysis. All single-molecule nanocatalysis was carried out in home-built flow cells, which were formed by double-sided tapes sandwiched between a quartz slide (Technical Glass) and a coverslip (Gold Seal). The solution was flowed into the cell with a flow rate of 10 $\mu L \cdot min^{-1}$. Before the assembly of a microflow cell, a certain amount of Au clusters in solution was dropped onto the slide, and incubated for about 30 minutes and then rinsed with large amount of water to wash away any unbound Au clusters (Scheme S1). A continuous-wave circularly polarized 532nm laser (CrystaLaser) of 1.5–3mW was focused onto an area of about 90×50 μm^2 on the sample to directly excite the fluorescence of the product resorufin. The fluorescence of resorufin was collected by a ×60 NA 1.2 water-immersion objective (Olympus), filtered by two filters (Chroma Technology) and projected onto an EMCCD camera (Andor Technology), which is controlled by Andor IQ software. The movies were analyzed using a home-written IDL program, which extracts the individual locations on which the fluorescent product molecules were formed and dissociated tandemly one-by-one across the entire movie. In order to avoid the possible effect from the deactivation of Au clusters during the catalysis, all movies were obtained only from the first 2 hours after the catalytic reaction started.

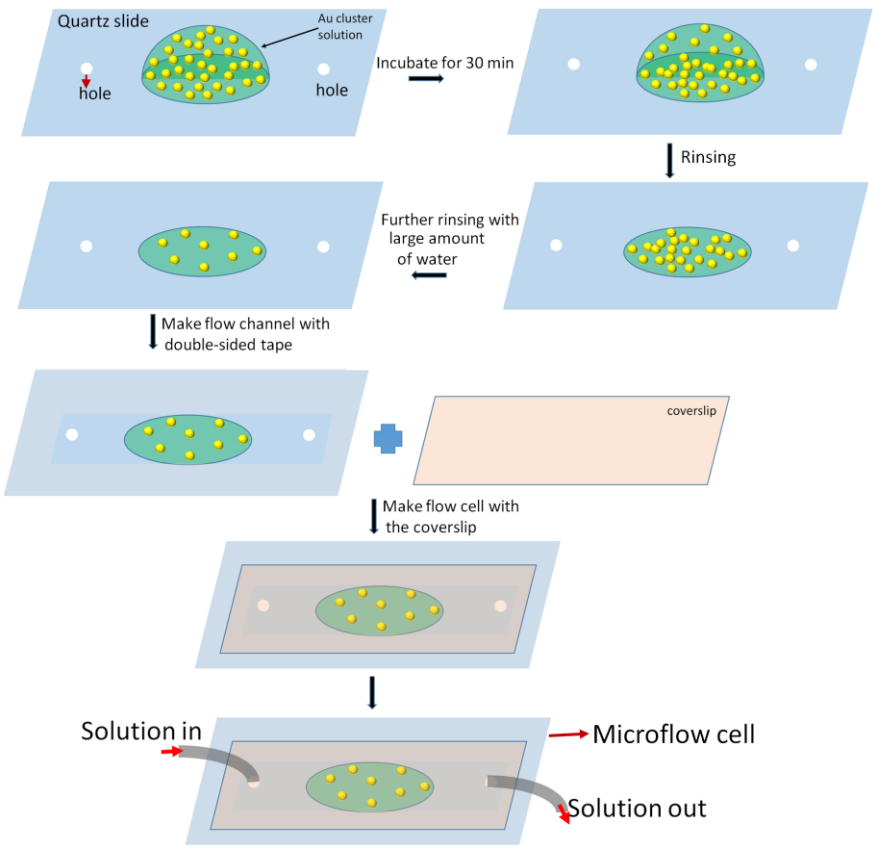

Scheme S1. Schematic illustration of the preparation of microflow cell for single molecule nanocatalysis.

2. Theoretical calculations about the adsorption of reactants and product on Au clusters.

In the present work, density functional tight-binding (DFTB) method with DFTB+ package was carried out to obtain the optimized structures for different sizes of Au clusters with full MPA ligands (Au_{15}, Au_{18} and Au_{25} in Fig. S1). Self-consistent charge density functional tight-binding (SCC-DFTB) formalism based on the second-order expansion of the Kohn–Sham total energy in DFT with respect to charge density fluctuation within the tight-binding framework is employed.[S3] Based on the optimized Au clusters, other structural models including reactants (substrate and NH_2OH) and product molecules were built on suitable sites, and NH_2OH molecules were placed close to substrate molecule successively. To obtain the interaction between reactant or product with or without NH_2OH and the Au clusters, the adsorption energy (E_{ad}) was estimated as the difference between the energy of formed complex (E_{Total}) and that of isolated moieties (E_A and E_B). In the current work, the adsorption energy (E_{ads}) was calculated based on the equation:

$$E_{ad} = E_{Total} - (E_A + E_B)$$

With this definition, a negative value corresponds to the stable adsorption on Au cluster surface.

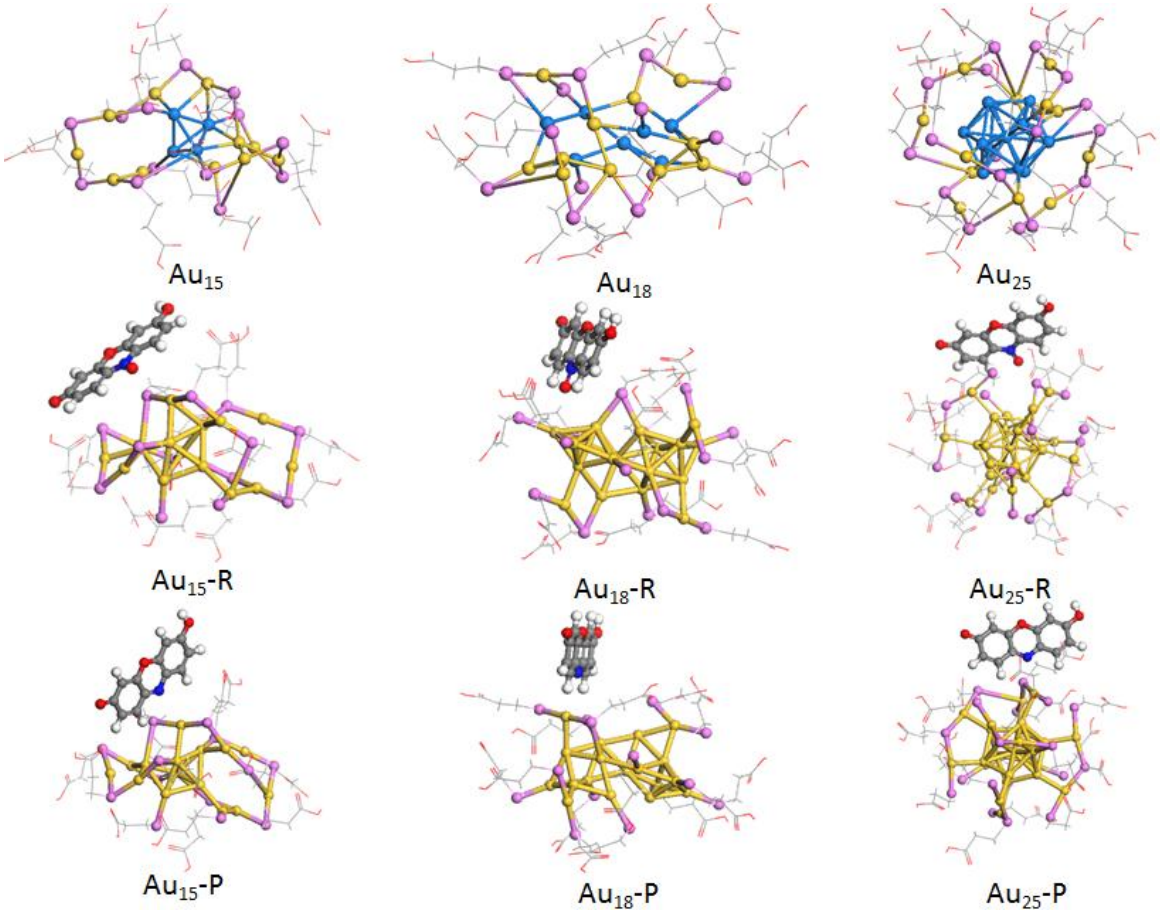

Fig. S1. The optimized structure models for Au cluster with MPA and the models with reactant (R, resazurin) and product (P, resorufin) adsorbed.

3. The roles and stability of MPA on Au clusters and the stability of Au clusters on slide during the catalysis.

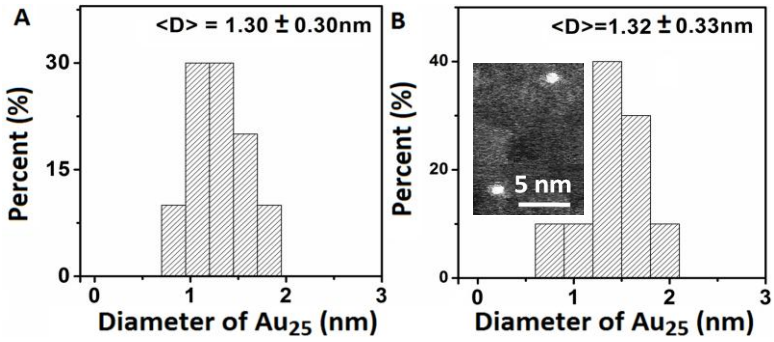

Fig. S2. The size distribution of Au_{25} before (A) and after (B) the long-term (6 hours) catalytic reduction reaction of resazurin by NH_2OH. The inset in (B) is the typical TEM image of Au_{25} clusters after the long-term catalytic process.

4. The sparse distribution of individual Au clusters on surface.

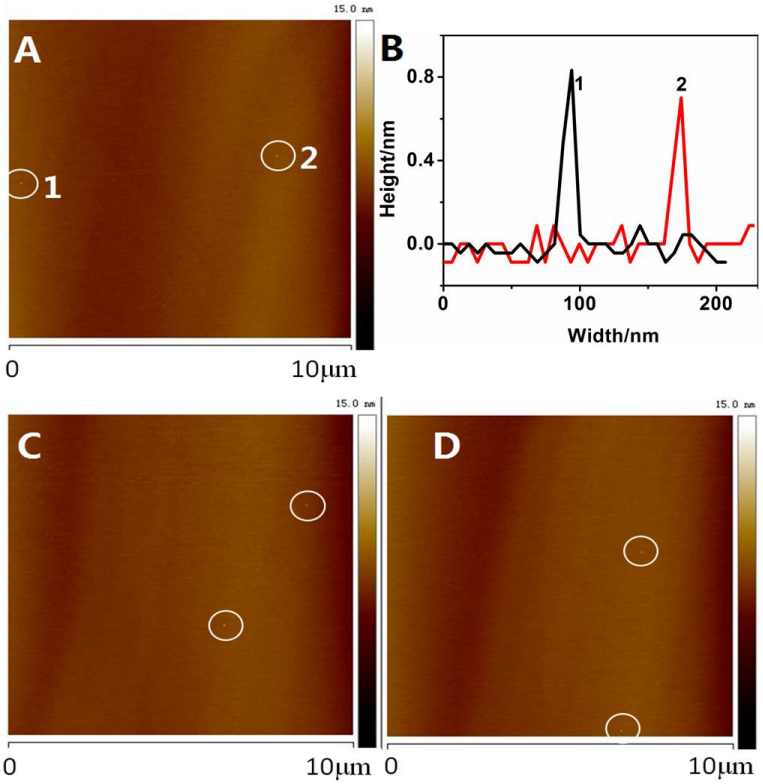

Fig. S3. Typical Atomic force microscopy (AFM) image (A, C, D) to show the sparse distribution of individual Au clusters (Au_{25}). The sample was prepared with a drop of dilute Au_{25} solution in the same concentration as that for the preparation of the microflow cell for single-molecule nanocatalysis and a subsequent water rinsing. (B) The height profiles for two typical Au_{25} clusters shown in (A) marked in circles.

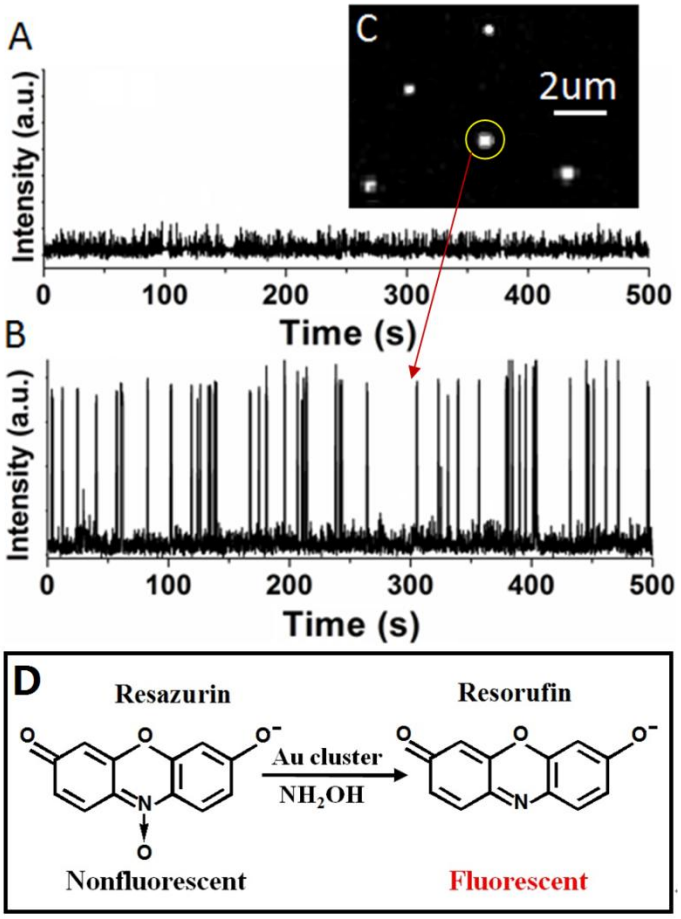

Fig. S4. (A) The background signal: a typical fluorescence trajectory from a random location in a blank flow cell without the deposition of nanocatalysts. (B) A digital fluorescence trajectory or trace from a single Au_{25} deposited on slide in the flow cell. It was obtained from the location on the slide indicated by the circle shown in (C). (C) A typical fluorescence image taken from an EMCCD camera to show the surface density of individual clusters on slide. (D)Au-cluster-catalyzed reduction of resazurin to fluorescent resorufin by NH_2OH in aqueous solution.

5. The effect of the interaction between Au clusters and the slide on the catalytic activity of Au clusters.

Due to the existence of -COOH on MPA, the interaction between the clusters and the quartz slide (SiO_2) could be very complex. Our experimental observations indicate that the Au clusters can be immobilized on the slide surface tightly indicated by the continuous observation of digital signal in a time window longer than 5 hours, as shown in Fig. S4B. Otherwise, if the individual Au clusters detached from the slide, the digital catalytic signal would suddenly disappear after some time.

Furthermore, in order to evaluate the effect of interaction between Au clusters and slide on the catalysis of Au clusters, firstly, we studied the activity of free Au clusters for the same catalytic reaction from ensemble level. By monitoring the catalytic product formation process of free Au_{18} from the fluorescence spectroscopy in a cuvette with [Resazurin]=12 nM and [NH_2OH]=20mM, we obtained the turnover number frequency (TOF)

of 0.152 ± 0.032 s^{-1} per free cluster; secondly, via the single-molecule nanocatalysis in a static microflow cell with [Resazurin]=12 nM and [NH_2OH]=20mM, we obtained the catalytic activity of individual Au_{18} clusters immobilized on quartz slide and finally obtained the TOF of 0.140 ± 0.023 s^{-1} per cluster (averaged from multiple individual clusters on slide). The small difference between these two TOF values indicates that the interaction between the quartz slide and the Au clusters only led to negligible effect on the catalytic activity of Au clusters, which is consistent with the known weak effect of the SiO_2 support on the catalytic activity of metal nanocatalysts.[S4]

6. The reductant concentration dependence of product formation rate on Au_{15}.

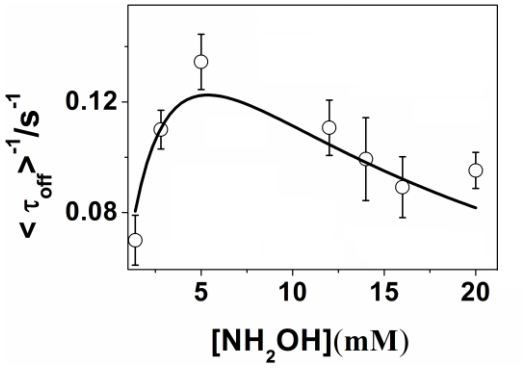

Fig. S5. Dependence of $<\tau_{off}>^{-1}$ on NH_2OH concentrations with a resazurin concentration fixed at 10 nM. Each data point is an average from the fluorescence turnover trajectories of >50 Au_{15} clusters.

7. Ruling out the contribution of Au_{15} deactivation to the observed decay of the product formation rates.

We carried out experiments to evaluate the stability of the catalytic activity of Au clusters during the catalysis. For instance, as shown in the following Fig. S6, for Au_{15} in the microflow cell with [resazurin]=10 nM and [NH_2OH]= 20 mM, there is no obvious observable variation of both $<\tau_{off}>^{-1}$ and $<\tau_{on}>^{-1}$ in the first 4 hours for both product formation and dissociation processes, indicating a remarkable stability of the clusters. Based on such fact, in the subsequent experiments, in order to avoid any possible effect from the deactivation of clusters, each point like that shown in Fig. 3A, C, D in the main text was obtained from the trajectories (like that shown in Fig. 1C) or movies obtained in the first 2 hours after the catalytic reaction started, as indicated in Fig. S6A. In this way, any possible deactivation effect of the clusters on $<\tau_{off}>^{-1}$ or $<\tau_{on}>^{-1}$ could be excluded, and we can then conclude that the observed decay of $<\tau_{off}>^{-1}$ for Au_{15} shown in Fig. 3C or Fig. S5 is not due to the deactivation of Au_{15} clusters.

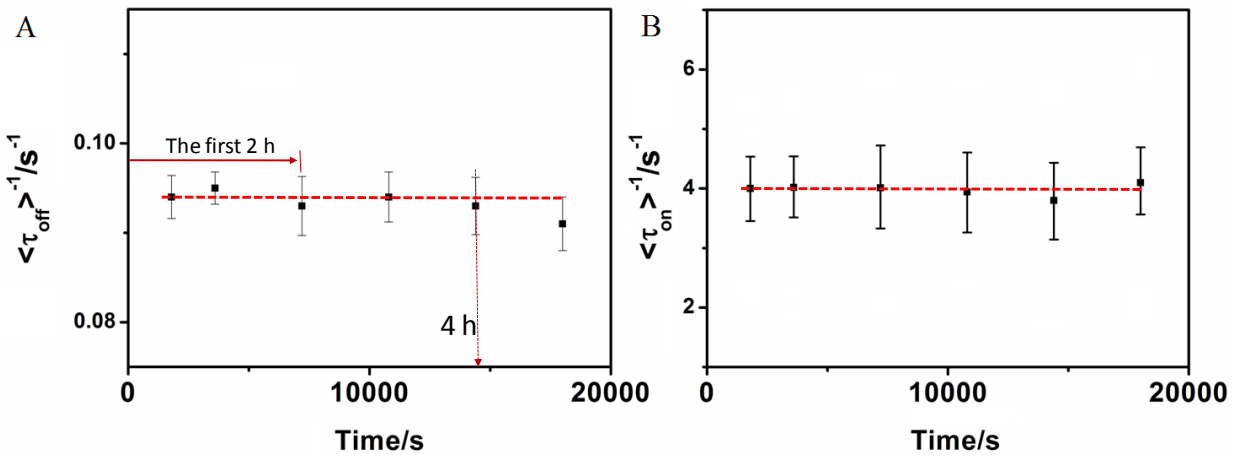

Fig. S6. The time-dependent rate of $<\tau_{off}>^{-1}$ (A) and $<\tau_{on}>^{-1}$ (B) averaged from >50 individual Au_{15} at 10 nM resazurin and 20 mM NH_2OH.

8. Ruling out the effect of ligand on the observed difference of catalytic properties of Au clusters

As for the observed difference of catalytic properties of Au clusters, in order to figure out whether such difference is from the ligand effect or not, we synthesized another type of Au clusters of $Au_{25}(MHA)_{18}$ (Fig. S7A) protected by 6-Mercaptohexanoic acid (MHA, $C_6H_{12}O_2S$) according to previous work.[S2] The chain of ligand MHA is much longer than that of the ligand 3-Mercaptopropionic acid (MPA, $C_3H_6O_2S$) on the studied Au clusters ($Au_{15}(MPA)_{13}$, $Au_{18}(MPA)_{14}$, and $Au_{25}(MPA)_{18}$). Furthermore, to see the possible effects of different ligands on the observed activities of Au clusters, we studied the catalytic behavior of individual $Au_{25}(MHA)_{18}$ for the same model reaction as that for $Au_{25}(MPA)_{18}$. Interestingly, as shown in the following Fig. S7B,C, the catalytic behavior of $Au_{25}(MHA)_{18}$ follows the same mechanism as that of $Au_{25}(MPA)_{18}$ (shown in Figure 3A,D in the manuscript): the product formation process follows the noncompetitive Langmuir−Hinshelwood mechanism, while the product dissociation rate is also independent of the substrate concentration. The obtained values of parameters are summarized in the following Table S1. As it shows, the obtained value of γ_{eff} or γ_{eff}/S on $Au_{25}(MHA)_{18}$ is slightly smaller than that on $Au_{25}(MPA)_{18}$, indicating that the longer molecular chain in MHA can slightly slowdown the reactivity of the surface sites on Au clusters. It also shows that the product dissociation (reflected by k_3) from the cluster $Au_{25}(MHA)_{18}$ is slightly slower than that on the cluster $Au_{25}(MPA)_{18}$, indicating that the longer molecular chain in MHA can slightly slowdown the product dissociation process from Au clusters. It should be noted here, since the chain-length of the ligand MHA is almost twice of the MPA, then the observed slight difference shown above indicates that these two parameters are not sensitive to the ligand.

Furthermore, Table S1 shows almost no difference between the adsorption abilities (α_B) of substrate resazurin on the same sized Au clusters but with different ligands, confirming that the parameter α_B, characterizing the binding ability of substrate resazurin on Au cluster, indeed can reflect the intrinsic binding ability of substrate on the surface of Au clusters and is also insensitive to the types of ligands.

In all, these results indicate that the observed difference of catalytic properties among clusters is not from the ligand effect, otherwise, these parameters would have varied hugely after the ligand was changed.

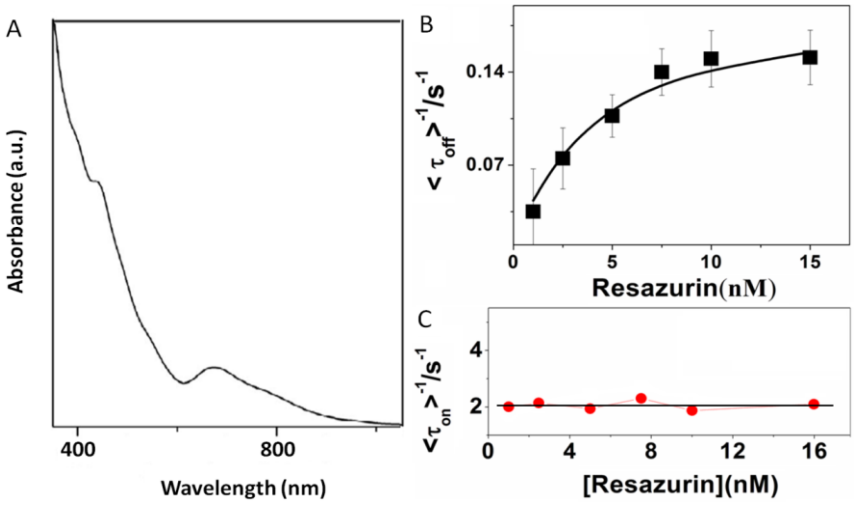

Fig. S7. (A) UV/Vis absorption of the as-synthesized nanocluster of $Au_{25}(MHA)_{18}$. (B) Resazurin concentration titrations of $<\tau_{of\ f}>^{-1}$ on $Au_{25}(MHA)_{18}$ with 20 mM NH_2OH. Each data point is averaged over the turnover trajectories of >50 clusters. Solid line is the fitting with Eq 1, with parameters summarized in the following Table RR1. (C) Resazurin concentration dependence of $<\tau_{on}>^{-1}$ of $Au_{25}(MHA)_{18}$.

9. X-ray photoelectron spectroscopic (XPS) measurements.

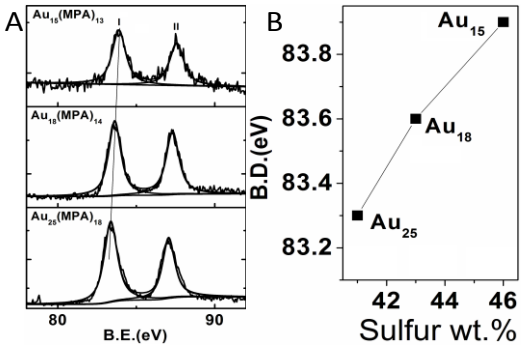

Fig. S8. XPS characterization of the Au_{4f} of $Au_{15}(MPA)_{13}$, $Au_{18}(MPA)_{14}$, and $Au_{25}(MPA)_{18}$.

10. Calculation of the Diameter of Au clusters.

If one counts the number of metal atoms per particle (Au_nL_m), the size range of 1-2nm is roughly equivalent to a range of n from ~10 to ~250 atoms. Note that the number of Au atoms per spherical cluster can be estimated by a simple relation, N=59 atoms/nm^3×4/3×π×(d/2)^3 nm^3, where d (in nm) is the diameter of cluster. This equation is derived from fcc (face centered cubic) gold, but it also can provide an accurate enough estimation even for non-fcc-structured Au nanoclusters.[S5] The Au core diameter (d) of Au NCs could be calculated based on it.

Table S1. Cluster-averaged kinetic parameters of different sized Au clusters

	d_{Au}(nm)	γ_{eff}(s^{-1})	γ_{eff}/S*10^3($s^{-1}nm^{-2}$)	α_B(μM^{-1})	α_A(μM^{-1})	k_3(s^{-1})	δ(eV)	W_d(eV)
Au_{15}	0.78	0.51±0.02	267±10	839±118	0.050±0.010	4.1±0.1	0.43	6.5
Au_{18}	0.84	0.23±0.01	104±5	333±53	--	3.5±0.1	0.35	6.4
Au_{25}	0.97	0.21±0.02	92±7	290±46	--	2.3±0.1	0.25	6.2
Au_{25}[b]	0.97	0.19±0.02	83±9	296±57	--	2.1±0.2		
Au NPs[a]	6.0±1.7	0.28±0.02	2.5±0.9	6±2	--	0±3		
Au NPs[a]	9.1±1.5	0.32±0.01	1.2±0.2	57±7	--	1.9±0.3		
Au NPs[a]	13.7±2.4	0.37±0.02	0.6±0.1	110±5	--	2.9±0.4		

[a]Values of the Au nanoparticles (NPs) were obtained from Ref. 6 for comparison. [b]Values are for $Au_{25}(MHA)_{18}$ obtained from the fittings shown in Fig. S7.

Table S2. Adsorption energy of reactant and product on Au clusters.

	^{a}E$_{ad}$/eV	**^{b}E$_{ad}$/eV**	**^{c}E$_{ad}$/eV**	**^{d}E$_{ad}$/eV**
Au_{15}	-0.549	-0.052	-0.068	-0.088
Au_{18}	-0.203	-0.345	-0.184	-0.169
Au_{25}	-0.190	-0.202	-0.219	-0.189
	^{e}E$_{ad}$/eV	**^{f}E$_{ad}$/eV**	**^{g}E$_{ad}$/eV**	**^{h}E$_{ad}$/eV**
Au_{15}	-0.180	-0.052	-0.025	-0.027
Au_{18}	-0.175	-0.103	-0.094	-0.068
Au_{25}	-0.439	-0.377	-0.302	-0.242

Note: **a,b, c** and **d** represent the adsorption energy for reactant resazurin with zero, one, two and three NH_2OH molecules around, respectively; **e, f, g** and **h** represent the adsorption energy for product resorufin with zero, one, two and three NH_2OH molecules around, respectively.

References

(S1) Yu Y, Chen X, Yao Q, Yu Y, Yan N, Xie J. *Chem. Mater.***2013**, *25*, 946-952.

(S2) Yuan X, Zhang B, Luo Z, Yao Q, Leong D, Yan N, Xie J. *Angew. Chem. Int. Ed*. **2014**, *53*, 4623-4627.

(S3) Elstner M, Porezag D, Jungnickel G, Elsner J, Haugk M, Frauenheim T, Suhai S, Seifert G. *Phys. Rev. B* **1998**, *58*, 7260-7269.

(S4) Nie X, Qian H, Ge Q, Xu H, Jin R. *ACS Nano* **2012**, 6, 6014-6022.

(S5) Jin R C, Qian H F, Wu Z, Zhu Y, Zhu M, Mohanty A, Garg N. *J. Phys. Chem. Lett.* **2010**, *1*, 2903-2908.